A 1 kHz A-Scan Rate Pump-Probe Laser-Ultrasound System for Robust Inspection of Composites

Ivan Pelivanov, Alex Shtokolov, Chen-Wei Wei, and Matthew O'Donnell, *Fellow, IEEE*

Abstract—We recently built a fiber-optic laser-ultrasound (LU) scanner for nondestructive evaluation (NDE) of aircraft composites and demonstrated its greatly improved sensitivity and stability compared with current noncontact systems. It is also very attractive in terms of cost, stability to environmental noise and surface roughness, simplicity in adjustment, footprint, and flexibility. A new type of a balanced fiber-optic Sagnac interferometer is a key component of this all-optical LU pump-probe system. Very high A-scan rates can be achieved because no reference arm or stabilization feedback are needed. Here, we demonstrate LU system performance at 1000 A-scans/s combined with a fast 2-D translator operating at a scanning speed of 100 mm/s with a peak acceleration of 10 m/s^2 in both lateral directions to produce parallel B-scans at high rates. The fast scanning strategy is described in detail. The sensitivity of this system, in terms of noise equivalent pressure, was further improved to be only 8.3 dB above the Nyquist thermal noise limit. To our knowledge, this is the best reported sensitivity for a noncontact ultrasonic detector of this dimension used to inspect aircraft composites.

I. Introduction

PUMP-PROBE laser ultrasound methods use laser generation of ultrasound (US) signals and their noncontact optical detection [1]–[4]. Laser-induced ultrasound has many advantages over conventional contact piezoelectric techniques because it does not require any contact with an object under study and can be used to generate different US modes (longitudinal [2], [5] and shear waves [2], [6], [7], surface or Lamb waves [2], [8]–[11] and, in particular cases, even guided waves [12]).

In our current work, laser-generated longitudinal US waves are employed. The directivity pattern of longitudinal waves is always normal to the sample surface independent of the angle at which the laser pulse irradiates the surface [2], [5]. When stress and thermal confinement conditions are satisfied [5], LU signals are ultra-wideband with a temporal profile usually consisting of only one or

two oscillations and, in some cases, mimicking the profile of the laser pulse envelope. Indeed, for the same characteristic frequency, the LU signal is at least 3 times shorter than the envelope of a conventional piezo-generated US signal. Therefore, at least 3 times better resolution at any fixed depth can be achieved or, alternatively, 3 times smaller characteristic frequency can be used to get the same resolution but at much greater depths.

Different optical schemes can be used for US signal detection. Several resonance-based optical detectors have been developed that can reach the sensitivity of the best piezoelectric transducers [13]–[17]. However, these schemes still require acoustic coupling.

All-optical noncontact methods have been used for NDT&E of composite materials for more than thirty years [1]–[4]. Different approaches, including those specially developed for composites, were proposed [9]–[11], [18]–[29]. The most interesting approaches demonstrated to date include confocal Fabry–Perot [1], [4], homodyne and heterodyne Mach–Zehnder [9]–[11], [22], [23], and Sagnac interferometers. The first two approaches require either stabilization or/and employ a reference arm. However, stabilization usually slows the maximum detection rate. Using a reference arm makes the system sensitive to speckle, surface roughness, and large parasitic displacements induced by thermal lens effects [30] in the excitation area at the composite surface. The Sagnac interferometer design is the most promising in our opinion for laser-ultrasound NDE of composites because of its robustness provided the sensitivity required for real applications can be delivered in a practical design. We note some seminal work on Sagnac interferometer development in [24]–[29]. For a more detailed discussion of interferometer designs for the NDE of composites, we refer to our previous work [31], [32]. To date, however, no noncontact techniques for US detection have approached the sensitivity of the best contact detectors nor the scan speed of conventional contact approaches.

We have recently demonstrated [31], [32] that an all-optical system for composite inspection can be greatly optimized. In particular, we have reduced the system footprint and the overall system cost to about $50k (including the laser cost, $20k, and the interferometer cost, ~$7k). In addition, this system is robust to environmental noise, with detection sensitivity comparable to that of the best piezoelectric transducers. A key component of our LU inspection systems is a fiber-optic Sagnac interferometer with

The authors are with the University of Washington, Department of Bioengineering, Seattle, WA 98195, USA (e-mail: ivanp3@uw.edu).

I. Pelivanov is also with Lomonosov Moscow State University, Physics Faculty, Moscow 119991, Russia.

a balanced detection scheme. The primary advantages of the Sagnac approach are:

- all interferometer components are fiber optic, which makes it very rugged and flexible;
- both interfering beams are formed by reflection of the probe beam from the same point on a sample surface (no reference arm is employed), making the scheme extremely stable to environmental noise and robust to surface roughness;
- very little internal noise induced by self-reflections between and inside fibers due to a low coherence source on receive (super luminescent diode with a coherence length of 40 μm);
- balanced detection removes all polarization-insensitive light, including a thermal lens signal during US signal generation;
- extremely easy to adjust by rotating pads on a polarization controller;
- detection sensitivity can be optimized within a desired bandwidth by changing the delay line (fiber) length.

Because no reference arm and, therefore, no time-consuming stabilization feedback, is employed in the interferometer, a very high A-scan rate can be potentially achieved in imaging. However, in our previous study, we used a low 15 Hz repetition rate for the pump laser, with translation at relatively slow rates limited to 8 mm/s. Indeed, when a low pulse repetition rate (PRR) is used, the irradiation limit is determined by the laser fluence, i.e., energy deposited to a unit area of the sample. For graphite-epoxy composites, it is about 100 mJ/cm². In the visible and near infrared ranges, this threshold depends very little on optical wavelength for nanosecond laser pulses because the main absorbance is provided by graphite fibers. However, when the laser PRR exceeds 100 Hz, heat released in the material starts to be accumulated from pulse to pulse and thereby dramatically reduces the exposure limit. Proper synchronization of lasing with sample motion, and automatic turn-off when motion is complete, allows high PRR operation at rates reaching the kilohertz level.

Here, we demonstrate a fast scanning system performing at least 1000 A-scans/s with an improved SNR and real-time visualization of B-scans, including data reception, signal processing, and imaging. Further details are provided in Section II.

II. METHOD

A. Samples of Fiber-Reinforced Composites

The LU system has inspected a large number of samples for flaw detection, material porosity assessment, wrinkle visualization, and evaluation of heat damage. Because of proprietary issues, these results cannot be presented at this time. However, here we demonstrate the overall capabilities of the system using two samples of fiber-reinforced graphite-epoxy composites provided by Boeing Research & Technology with typical flaws found in real composite parts. We note that the system can be used for many diagnostic purposes for which contact-free, submillimeter axial resolution, and high-speed measurements are needed.

Composite samples were not transparent for both pump and probe light. No special preparation of the composite surface had been made before measurement; thus, detection was performed from the actual sample surface. Both 19-ply samples had a thickness of 3.6 mm (longitudinal wave sound speed is very close to 3000 m/s, volume density is about 1600 kg/m³). Artificial inclusions, made from a 20-μm-thick brass foil, tape, and polymer material, were embedded in the sample structure. One of the samples with inclusions located close to the middle of its depth was used for imaging (see Section III-B); the second sample with the inclusions close to the front surface was used to demonstrate real-time system operation (see Section IV). More details on composite samples can be found in [31] and [32].

B. Measurement Scheme

Here, we use a scheme very common in LU flaw detection. Briefly, pulsed laser radiation (i.e., pump) is focused to a few-millimeter-scale spot on the front surface of the composite sample, where it is absorbed. High optical absorption (more than 200 cm⁻¹) of the graphite-epoxy composite sample creates an ultra-wide band acoustic transient [optoacoustic (OA) signal] through thermal expansion [5]. A low coherent continuous wave (CW) source, super luminescent diode (SLD), is used for noncontact detection (i.e., probe) of OA signal components backscattered by the composite structure (the detailed information on the SLD can be found in [31] and [32]). Data recorded at one transmit/receive position produces an A-scan; scanning along a line creates a B-scan and a snaking trajectory can be used to acquire multiple B-scans forming a complete 3-D data set. Data from the complete 3-D acquisition can be rearranged to extract in-plane distributions of the backscattered signal amplitude (i.e., C-scans).

C. Fast Scanning Pump-Probe System

As mentioned, the advantage of the system described here over that previously demonstrated in [31] and [32] is its fast scanning performance, enabling 1000 A-scans/s acquisition with real-time B-scan image reconstruction in parallel. A custom-designed 2-D XY translation platform (Aerotech Inc., Pittsburgh, PA, USA; http://www.aerotech.com) was employed with the pump-probe system. The composite sample was fixed on the translation platform, which could be moved at a linear translation speed of 100 mm/s with a peak acceleration of 10 m/s² in both lateral directions.

To maintain high image resolution in the lateral directions at high translation speeds, the pump laser must operate at high pulse repetition rates (500 Hz and higher).
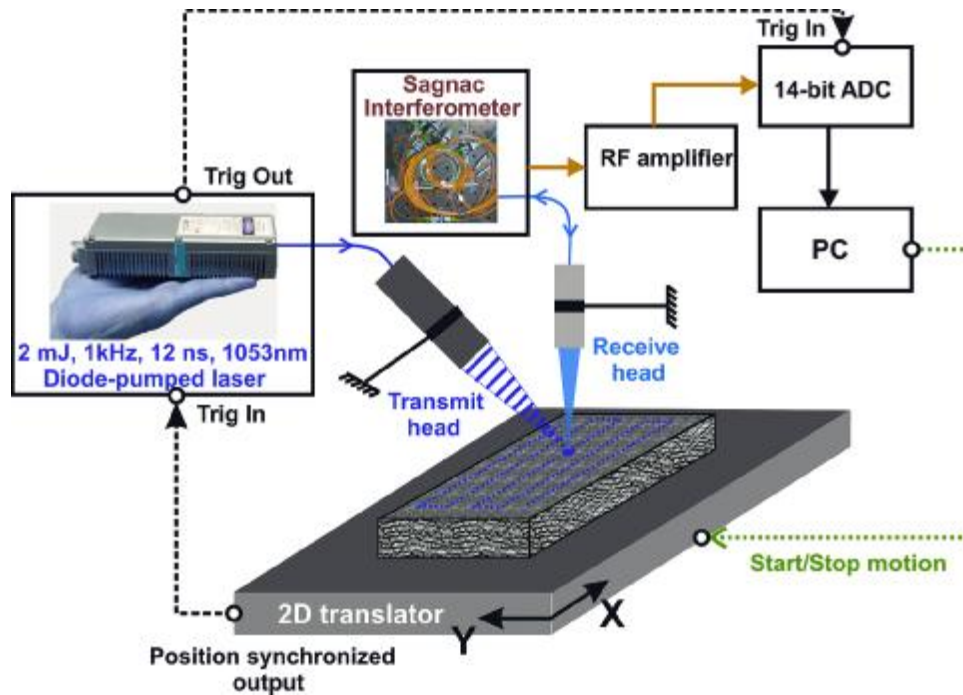
Fig. 1. Block-diagram of the LU scanner. Transmit and receive heads are fixed while the sample is moved with a 2-D translation platform (100 mm/s maximum translation speed). The position-synchronized output of the translator triggers pump laser firing with reference to the spatial coordinate and turns lasing on and off when scanning starts and stops. This approach enables a PRR of 1 kHz with precise A-scan intervals but without overheating the composite sample.

However, damaging the sample by overheating is possible if sample translation is not properly synchronized with lasing. To avoid damage, the laser must be turned off when the sample is not moving. In addition, the laser energy deposited into a unit sample surface per unit time (laser intensity) should be below the heat damage threshold. Simple synchronization of shutting the laser on/off with start/stop instants of sample motion does not completely solve the problem because of acceleration/deceleration phases in translation. Furthermore, if the laser PRR is kept constant, the interval between A-scans will change while the sample is accelerated/decelerated.

A position-synchronized output of the translation platform helped solving these issues. A complete block diagram of overall system synchronization is shown in Fig. 1. A Z820 workstation (Hewlett-Packard Co., Palo Alto, CA, USA; http://www.hp.com) is used for LU system operation through a LabView interface (National Instruments Corp., Austin, TX, USA). The software sets the speed of motion in the interval of (0.01 to 100) mm/s for both lateral (X and Y) directions as determined by the geometry of the scanning trajectory. The transmit and receive heads are fixed while the sample is moved with a 2-D translator. Laser firing is triggered based on the coordinate (see Fig. 1). i.e.. based on the spatial, not time, interval between firings. The A-scan stepping accuracy is better than 1 μm over the whole scanning length, including acceleration/ deceleration regions. Immediately after triggering, the laser (Model Tech 1053 Advanced, Laser Export Co. Ltd., Moscow, Russia; http://www.laser-export.com) fires and sends a trigger signal to the ADC (Model Razor Compu-

scope RZE-002–300, GaGe, DynamicSignals LLC, Lockport, IL, USA: http://www.gage-applied.com) to start data acquisition. The jitter between laser firings was better than 2 ns, which is negligibly small for the experiments reported here.

This approach can acquire 1000 A-scans/s at 100 mm/s scanning speed in both lateral directions. A fast algorithm performed data acquisition, processing, and imaging in parallel to scanning, making it possible to reach true real-time B-scan imaging. Again, no stabilization of the interferometer was used and, therefore, image frame rates can be further increased.

The laser beam spot was optimized to reduce acoustic diffraction effects (diffraction length is proportional to the square of the laser beam diameter) while simultaneously producing an optoacoustic (OA) signal of sufficient amplitude (inversely proportional to the square of the laser beam diameter). Thus, the laser beam diameter was chosen to be 1.5×2 mm (being elliptical because of the oblique incidence of the pump laser beam relative to the sample surface) for 3-mm-thick samples. Incident pumplaser pulses are delivered at an oblique angle ($\sim 40°$ from the sample normal), allowing the probe-laser beam to be focused to the same point on the sample surface. The OA-generated pulse propagates through the sample, partially reflecting off of the composite structure and reflecting off of the back wall. All acoustic waves propagating back to the front wall of the sample are detected with the fiber-optic Sagnac interferometer [31], [32], which is a key component of our inspection system. RF signals output from the interferometer are amplified in the frequency range of 1 to
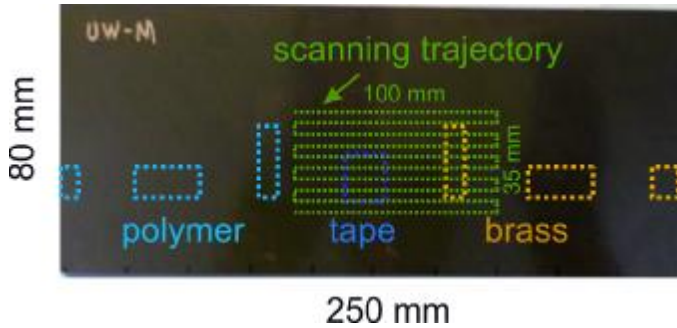
Fig. 2. Diagram of the composite sample (UW-M). Dashed rectangles represent the inclusions, their size, and location. The green snaking curve corresponds to the scanning trajectory, consisting of 36 B-scan frames, each 100 mm long, stepped by 1 mm intervals. Each B-scan consists of 1000 A-scans, recorded with a step of 0.1 mm. The sample is fixed to the XY translator, which provides motion at a speed of 100 mm/s in both directions. A 1 kHz pulse repetition rate of lasing produces a B-scan recording time of 1 s and less than 40 s for complete 3-D scanning of the entire 100 × 35 mm (X and Y directions) region.

10 MHz by an amplifier (Model 5072PR, Panametrics, GE Measurement and Control, Billerica, MA, USA), digitized to 14 bits by the PCI Express3 ADC and transferred to the workstation for further signal processing and display.

The current LU system has a few important advantages compared with the one used in our previous work [31], [32]. First, fast (100 mm/s) 2-D translation fully synchronized with lasing is used instead of a slow 1-D linear translator. Second, a new diode-pumped laser operating at 1053 nm with only 0.1% pulse-to-pulse energy variability, almost perfect Gaussian spatial and temporal profiles, a 12 ns pulse duration, and more than 2 mJ laser energy at 1 kHz emission is used. This laser also has a very user-friendly interface with trigger input and outputs, enabling both external and internal trigger modes and variable pulse repetition rates. Finally, new software has been developed to perform the whole cycle of measurement (data acquisition, signal processing, imaging, and saving) in real time.

D. Scanning Diagram

Fig. 2 shows a diagram of measurements made on a single composite test sample. A set of B-scans were recorded along the snaking trajectory depicted by the dashed line. The sample was translated at the maximum allowed speed of 100 mm/s for both X and Y directions. All 36 B-scans consist of 1000 A-scans, covering a 100 mm distance in the X-direction and were equally spaced by 1 mm from each other in the Y-direction. All other operations needed to produce images, including data processing, data storage, and final B-scan representation, were performed simultaneously with sample motion; that is, no extra time was required between B-scans and image display in a truly real-time mode. Software written using LabView allowed full control of the imaging process, including the choice of scan speed and scanning interval by both axes, as well as complete signal processing and image representation with many options.

III. RESULTS

A. A-Scan Signals

A 14-bit ADC was used for RF signal detection; a LabView interface provided signal profiles and spectra and performed all signal processing required for real-time B-scan imaging in parallel to recording data. In addition, RF signals from the balanced detector were also captured with a digital oscilloscope (TDS 1002, Tektronix, Beaverton, OR, USA) to visualize the high-SNR RF signals produced during scanning.

Fig. 3(a) shows a typical temporal profile for an OA signal (A-scan), recoded in the region without visible defects in the structure. Its first positive peak corresponds to the OA signal generated at the front sample surface caused by absorption of pulsed laser radiation. All transients recorded at later times correspond to reflections from inside the composite structure. Note that eighteen oscillations corresponding to a 19-ply (layer) structure are clearly seen between front- and back-wall signals. The presence of the defect is quite evident on the signal profile as well as its second- and third-order reverberations (within 4 µs time window) [see Fig. 3(b)].

Both RF profiles illustrated in Fig. 3 were obtained in a single-laser-shot regime, i.e., no averaging was applied. As seen, the signal amplitude is much higher than the noise floor; an estimated SNR, computed as the ratio of the front-wall OA signal to the noise pressure, is no worse than 40 dB within a 1 to 10 MHz frequency range. In comparison with our previous results, installing a very stable diode-pumped laser to the system made it possible to further improve the noise figure of the whole LU system and decrease it to only 8.3 dB above the Nyquist thermal noise limit, the ultimate value which cannot be overcome. The procedure for determining the noise figure used a fully calibrated, wide-band PVDF detector, as described in detail in [31] and [32].

B. B-Scan Images

As mentioned earlier, the snaking scanning trajectory consisted of 36 B-scan frames (1000 A-scans each) separated by 1 mm, corresponding to a 100 × 35 mm (according to X- and Y-directions) scanning region. All A-scans were normalized by their amplitudes at the front surface to avoid signal fluctuations related to surface roughness and possible local fluctuations of the light absorption coefficient. Note that such fluctuations, about 20% of the amplitude, do not change the signal profile.

Sample motion was performed at a constant speed of 100 mm/s for both axes. A-scans were stepped by (0.1 ± 0.001) mm. The high accuracy of A-scan stepping was enabled by a field-programmable gate array (FPGA) within the translator motor to trigger the laser precisely referenced to the coordinate. Signal processing was performed in parallel to scanning, adding no extra delays in the pro-
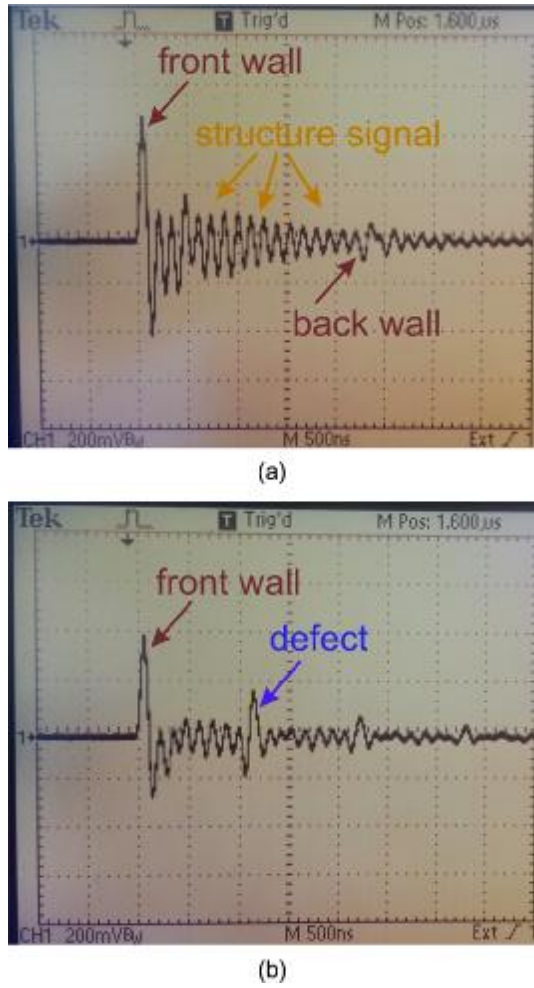
Fig. 3. Typical temporal profiles of A-scans recorded in the region (a) without and (b) with an artificial inclusion (20-µm-thick brass foil) in the sample structure. For the latter case, a signal reflected from the inclusion as well as its second- and third-order reverberations are clearly seen within a 4 µs time window.

cedure and providing truly real-time diagnostic images limited only by the translation speed.

Fig. 4 presents a movie of all 36 B-scan frames playing at a frame rate of 1 frame/s (the same rate as they appear during scanning). The upper movie panel corresponds to full 1 to 10 MHz bandwidth recording and the lower one includes an additional post-processing step of low-pass filtering (LPF) with a cutoff frequency of 5 MHz. Six of those B-scans separated by 7 mm are also shown as static full bandwidth images [Figs. 4(a)–4(f)] and LPF images [Figs. 4(g)–4(l)]. All the B-scan images illustrated in Fig. 4 were obtained in a single-shot regime, i.e., no averaging was applied. Clearly, the sensitivity of the Sagnac detector is sufficient for noncontact imaging of the composite materials used in this study even in a single-shot regime. Because the lateral resolution generally (without applying an additional spatial deconvolution procedure [33]) cannot be better than the pump laser beam diameter, 1.5 mm in our case, and the scanning step is only 100 µm, a simple moving average filter can be applied in the translation (X)

direction to further improve the SNR, if needed. Moving average filtering can also be applied in two (X and Y) dimensions for three-dimensional data acquisition. Note, that moving average filtering does not need extra data and does not change the acquisition and processing time.

The full bandwidth [upper panel of the B-scan movie 🖼 and Figs. 4(a)–4(f)] can help to visualize not only defects but the composite layered structure as well. This is a key feature of ultra-wideband LU detection which can be used to characterize the inherent structure of the composite itself to locate structure changes, such as wrinkles. As seen here, the layers are not perfectly flat. Figs. 4(a) and 4(f) are the first and last B-scan frames which correspond to regions with no inclusions embedded into the structure. Figs. 4(b)–4(e) correspond to scanning either through one [Figs. 4(b) and 4(e)] or two inclusions [Figs. 4(c) and 4(d)]. Because the inclusions are very thin (20 µm in thickness), they do not totally block propagation of ultrasound (US) through them, producing a partial US reflection. This is why US reflections from artificial structure inclusions are interleaved with US reflections from individual layers of the sample structure. The brass foil inclusion (which is centered at X $\cong$ 73 mm) is clearly seen as embedded into the structure. Another inclusion, a layer of tape (which is centered at X $\cong$ 34 mm), had a much lower impedance mismatch with that for the composite and, thus, is almost fully masked by the structure signal.

The power of wideband detection is that band-pass filtering can be applied to the detected signals to maximize the response in a desired frequency range. As we previously showed in [31], [32], the structure signal has a very narrow peak in the Fourier domain at about 7.2 MHz frequency, which can be filtered out. A super-Gaussian low-pass filter

$$\text{LP\_Filter}(f) = \exp(-(f/f_{1\text{LP}})^2 - (f/f_{2\text{LP}})^4), \qquad (1)$$

with characteristic frequencies f_1 and f_2 of $f_{1\text{LP}} = 5$ MHz and $f_{2\text{LP}}/f_{1\text{LP}} = 1.1$ was applied to full band-width signals to clear the structure signal. The bottom panel of the B-scan movie (🖼) shows LPF images, six snapshots of which are shown as static images in Figs. 4(g)–4(l). Clearly, the strong, periodic structure signal is mostly removed from all B-scans and US signal reflections corresponding to the defects are seen more clearly. In addition, large-scale structure imperfections which were hardly visible in full bandwidth images have become very clear. For example, small pores and structure imperfections near embedded large inclusions are clearly seen in Figs. 4(h)–4(l); a honeycomb structure is also evident in the near field and multiple reverberations even for the tape inclusion are well recognizable. On the other hand, the axial resolution has been degraded, resulting in blurring of defect signals and loss of high-frequency information. More robust methods that can minimize the periodic structure signal while maintaining more of the overall signal bandwidth will be the subject of future studies.
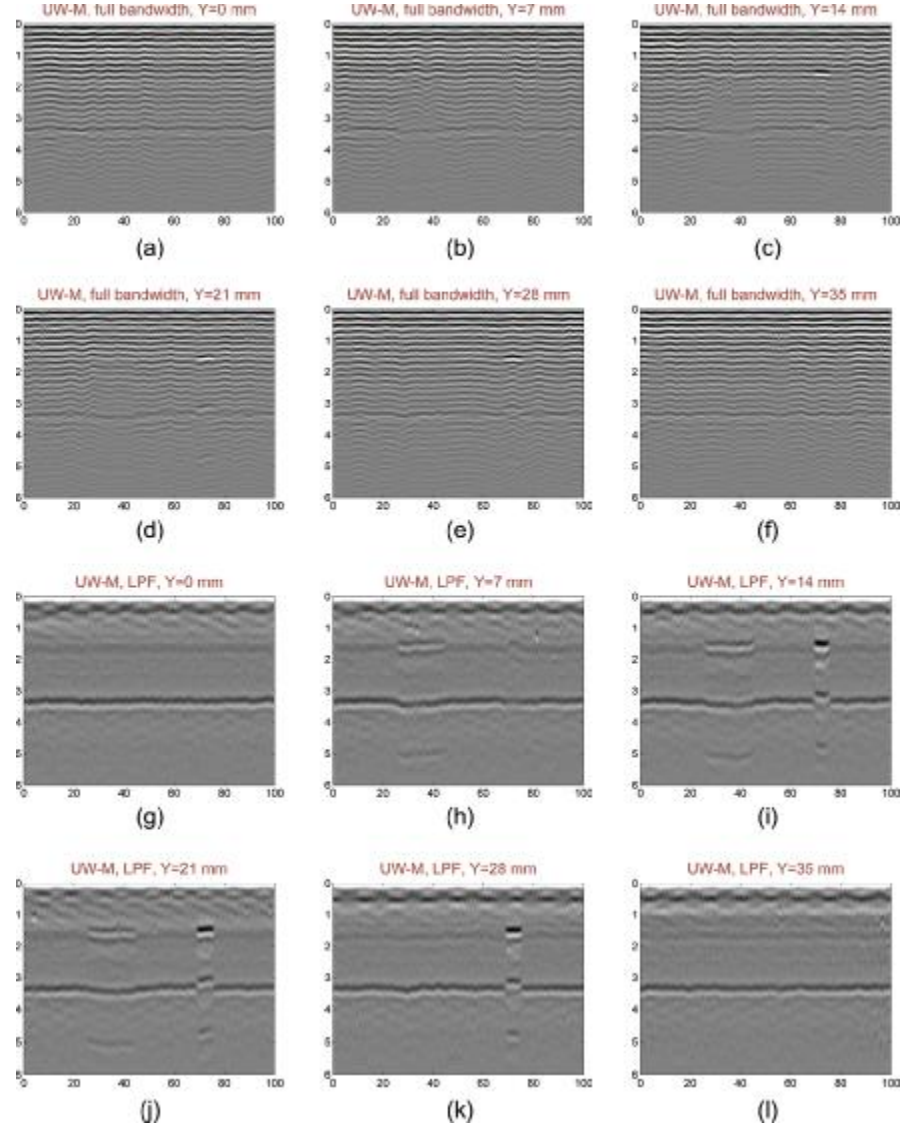
Fig. 4. Six equally spaced B-scan frames (snapshots of the B-scan movie ▶) are shown as static B-scan images for the (a)–(f) full bandwidth and (g)–(l) LPF processed. The spatial scale of both axes is shown in millimeters.

IV. DISCUSSION

Detection sensitivity is a key parameter for remote US measurements, because the sensitivity of optical interferometers is usually much worse than that of piezoelectric transducers. In our previous studies [31], [32], we showed a good 26 dB SNR and compared contact US measurements (using an ultra-wideband PVDF detector made from a 28-μm PVDF film) to equivalent measurements using the Sagnac detector. That allowed us to evaluate the detection system noise figure, 12.3 dB (i.e., noise level above the Nyquist thermal noise limit, the ultimate value which cannot be overcome). In this paper, we have improved detection sensitivity to 8.3 dB over the Nyquist noise floor mainly because of the increased temporal stability of the new diode-pumped laser source.

Another significant improvement has been obtained by integrating a fast scanning system with the high-repetition-rate pump laser. We demonstrate here real-time

scanning, acquiring at least 1000 A-scans/s, performing sample translation with 100 mm/s rates in both lateral directions, and visualizing B-scans in parallel to scanning. The precise position output of the translator triggers laser pulse emission to permit high accuracy A-scan stepping (∼1 μm) even for acceleration and deceleration regions. The step between A-scans under these conditions is 0.1 mm, which is probably not required. Because a reasonable laser beam diameter for flaw detection in samples with the thickness larger than 1 mm should be bigger than a few millimeters (because of US beam diffraction spread), the step between A-scans can be increased to at least 1/3 of the laser beam spot size. Thus, translation at about 1 m/s would keep the same lateral resolution. In other words, the translation system can be significantly speeded up using the LU system presented here to match the requirements of specific composite inspection applications.

A 1-kHz laser PRR is not a physical limit in our approach because stabilization of the interferometer is not

required. As soon as lasing is synchronized with sample motion, the laser PRR can be properly chosen based on the irradiation threshold for the material being inspected. In our particular case, we performed signal processing and data saving in parallel to recording data. Moreover, RF signals (not final images) are stored. In other words, further increases in laser PRR are limited mostly by the time required to store RF data. The system presented here is good for research, but can be greatly optimized for field applications given that the laser PRR can operate in the multi-kilohertz range as long as proper scanning and data capture systems are developed in parallel.

A short video demonstrating real-time operation of the LU system can be seen in the system operation movie (▣). Note the very compact footprint of the pump laser and the very flexible interferometer design consisting of the fiber-optic components only.

In addition to the simple flaw detection experiments demonstrated in this work, we have already obtained many results for more complicated cases, including material porosity evaluation, and detection of wrinkles or heat damage, which are difficult to obtain with other techniques. These results will be published as soon as relevant IP is protected. We also intend to adopt the technology developed for NDE of composites to study metals for which a high-sensitivity, point-like detector can be a key element to precisely evaluate residual stress. The fast LU scanner described here has been recently replicated at Boeing and is now under test for field applications. Finally, we have identified some potential biomedical applications for the system.

V. CONCLUSIONS

The performance of a fiber-optic LU scanner for NDT and evaluation of composite materials has been demonstrated at a high 1000 A-scans/s imaging rate combined with a fast 2-D translator allowing sample movement with a scanning speed of 100 mm/s and a peak acceleration of 10 m/s^2 in both lateral directions. A position-synchronized output of the 2-D translator triggers laser firing, referencing all measurements to the current sample coordinate and providing a constant precise step between A-scans even for acceleration/deceleration regions. The detection sensitivity, in terms of the noise equivalent pressure, has been further improved to be only 8.3 dB above the Nyquist thermal noise limit. To our knowledge, this is the best reported sensitivity for a noncontact ultrasonic detector of this dimension. The fast LU scanner described here has been recently replicated at Boeing and is now under test for field applications.

ACKNOWLEDGMENTS

REFERENCES

[1] J.-P. Monchalin. "Optical detection of ultrasound." *IEEE Trans. Ultrason. Ferroelectr. Freq. Control*, vol. UFFC-33, no. 5, pp. 485–499, 1986.

[2] C. B. Scruby and L. E. Drain, *Laser-Ultrasonics: Techniques and Applications*. Bristol, UK: Adam Hilger, 1990.

[3] R. J. Dewhurst and Q. Shan, "Optical remote measurement of ultrasound," *Meas. Sci. Technol.*, vol. 10, no. 11. pp. R139–R168, 1999.

[4] J. P. Monchalin, "Laser-ultrasonics: From the laboratory to industry," in *Review of Progress in Quantitative Nondestructive Evaluation, 23A, AIP Conf. Proc.*, 2004, vol. 700, pp. 3–31.

[5] V. E. Gusev and A. A. Karabutov, *Laser Optoacoustics*, AIP, New York, 1993.

[6] D. A. Hutchins and D. E. Wilkins. "Polarized shear waves using laser line sources and electromagnetic acoustic transducer detection," *Appl. Phys. Lett.*, vol. 47. no. 8, pp. 789–791, 1985.

[7] C. Rossignol, J. M. Rampnoux. M. Perton, B. Audoin, and S. Dilhaire, "Generation and detection of shear acoustic waves in metal submicrometric films with ultrashort laser pulses," *Phys. Rev. Lett.*, vol. 94, no. 16, art. no. 166106, 2005.

[8] A. M. Aindow, R. J. Dewhurst, and S. B. Palmer, "Laser-generation of directional surface acoustic wave pulses in metals," *Opt. Commun.*, vol. 42, no. 2, pp. 116–120, 1982.

[9] H.-C. Wang, S. Fleming, and Y.-C. Lee, "A remote, nondestructive laser ultrasonic material evaluation system with simplified optical fibre interferometer detection." *J. Nondestruct. Eval.*, vol. 28, no. 2, pp. 75–83, 2009.

[10] D. Royer and C. Chenu, "Experimental and theoretical waveforms of Rayleigh waves generated by a thermoelastic laser line source," *Ultrasonics*, vol. 38, no. 9, pp. 891–895. 2000.

[11] F. Faese, F. Jenot, M. Ouaftouh, M. Duquennoy, and M. Ourak. "Fast slot characterization using laser-ultrasonics and mode conversion," *Meas. Sci. Technol.*, vol. 24. no. 9, art. no. 095602, 2013.

[12] H. Lee, H. Park, H. Sohn, and B. Kwon, "Integrated guided wave generation and sensing using a single laser source and optical fibers." *Meas. Sci. Technol.*. vol. 21, no. 10, art. no. 105207, 2010.

[13] C.-Y. Chao, S. Ashkenazi, S.-W. Huang, M. O'Donnell, and L. J. Guo, "High-frequency ultrasound sensors using polymer microring resonators," *IEEE Trans. Ultrason. Ferroelectr. Freq. Control*, vol. 54, no. 5, pp. 957–965, 2007.

[14] B.-Y. Hsieh, S.-L. Chen, T. Ling, L. J. Guo, and P.-C. Li, "All-optical scanhead for ultrasound and photoacoustic dual-modality imaging," *Opt. Express*, vol. 20. no. 2, pp. 1588–1596, 2012.

[15] T. Ling, S.-L. Chen. and L. J. Guo, "Fabrication and characterization of high-Q polymer micro-ring resonator and its application as a sensitive ultrasonic detector," *Opt. Express*. vol. 19. no. 2. pp. 861–869, 2011.

[16] A. Rosenthal, D. Razansky, and V. Ntziachristos, "Wideband optical sensing using pulse interferometry," *Opt. Express*, vol. 20, no. 17. pp. 19016–19029, 2012.

[17] E. Zhang. J. Laufer, and P. Beard. "Backward-mode multiwavelength photoacoustic scanner using a planar Fabry–Perot polymer film ultrasound sensor for high-resolution three-dimensional imaging of biological tissues," *Appl. Opt.*, vol. 47, no. 4, pp. 561–577. 2008.

[18] J.-P. Monchalin, "Optical detection of ultrasound at a distance using a confocal Fabry–Perot interferometer," *Appl. Phys. Lett.*, vol. 47, no. 1, pp. 14–16. 1985.

[19] A. Blouin and J.-P. Monchalin, "Detection of ultrasonic motion of a scattering surface by two-wave mixing in a photorefractive GaAs crystal," *Appl. Phys. Lett.*. vol. 65, no. 8. pp. 932–934, 1994.

[20] A. Blouin. C. Padioleau, C. Neron, and J.-P. Monchalin. "Differential confocal Fabry–Perot for the optical detection of ultrasound." in *Review of Progress in Quantitative Nondestructive Evaluation*, 2007. vol. 26, pp. 193–200.

[21] A. Blouin, L. Pujol, and J.-P. Monchalin, "Laser-ultrasonic testing system," U.S. Patent No. 6 813 951 B2, Nov. 9, 2004.

[22] A. Hochreiner, J. Bauer-Marschallinger, P. Burgholzer, B. Jakoby, and T. Berer, "Noncontact photoacoustic imaging using a fiber based interferometer with optical amplification," *Biomed. Opt. Express*, vol. 4, no. 11, pp. 2322–2331, 2013.

[23] S. J. Park, J. Eom, Y. H. Kim, C. S. Lee, and B. Ha Lee, "Noncontact photoacoustic imaging based on all-fiber heterodyne interferometer," *Opt. Lett.*, vol. 39, no. 16, pp. 4903–4906, 2014.

[24] B. Culshaw, "The optical fibre Sagnac interferometer: An overview of its principles and applications," *Meas. Sci. Technol.*, vol. 17, no. 1, pp. R1–R16, 2006.

[25] P. A. Fomitchov, S. Krishnaswamy, and J. D. Achenbach, "Compact phase-shifted Sagnac interferometer for ultrasound detection," *Opt. Laser Technol.*, vol. 29, no. 6, pp. 333–338, 1997.

[26] T. S. Jang, S. S. Lee, B. Kwon, W. J. Lee, and J. J. Lee, "Noncontact detection of ultrasonic waves using fiber optic Sagnac interferometer," *IEEE Trans. Ultrason. Ferroelectr. Freq. Control*, vol. 49, no. 6, pp. 767–775, 2002.

[27] T. S. Jang, J. J. Lee, D. J. Yoon, and S. S. Lee, "Noncontact detection of laser-generated surface acoustic waves using fiber optic Sagnac interferometer," *Ultrasonics*, vol. 40, no. 1–8, pp. 803–807, 2002.

[28] T. Tachizaki, T. Muroya, O. Matsuda, Y. Sugawara, D. H. Hurley, and O. B. Wright, "Scanning ultrafast Sagnac interferometry for imaging two-dimensional surface wave propagation," *Rev. Sci. Inst.*, vol. 77, no. 4, art. no. 043713, 2006.

[29] T. Buma and M. O'Donnell, "One-dimensional ultrasound receive array using spectrally encoded optical detection," *Appl. Phys. Lett.*, vol. 85, no. 24, pp. 6045–6047, 2004.

[30] S. J. Sheldon, L. V. Knight, and J. M. Thorne, "Laser-induced thermal lens effect: A new theoretical model," *Appl. Opt.*, vol. 21, no. 9, pp. 1663–1669, 1982.

[31] I. Pelivanov, T. Buma, J. Xia, C.-W. Wei, and M. O'Donnell, "A new fiber-optic noncontact compact laser-ultrasound scanner for fast NDT&E of aircraft composites," *J. Appl. Phys.*, vol. 115, no. 11, art. no. 113105, 2014.

[32] I. Pelivanov, T. Buma, J. Xia, C.-W. Wei, and M. O'Donnell, "NDT of fiber-reinforced composites with a new fiber-optic pump-probe laser-ultrasound system," *Photoacoustics*, vol. 2, no. 2, pp. 63–74, 2014.

[33] Y. Wang, D. Xing, Y. Zeng, and Q. Chen, "Photoacoustic imaging with deconvolution algorithm," *Phys. Med. Biol.*, vol. 49, no. 14, pp. 3117–3124, 2004.

Ivan Pelivanov is the Assistant Professor at the Physics Faculty of M. V. Lomonosov Moscow State University and visiting Assistant Professor at the University of Washington. He graduated from the group of Prof. A. A. Karabutov, which is a pioneering and renowned team in various physical and biological applications of optoacoustic spectroscopy, and he received his Ph.D. degree in 2000. His recent research focuses on designing sensitive wideband contact and noncontact detectors, application of optoacoustic methods in NDT and material evaluation, analytic chemistry, and medicine.

Alex Shtokolov received the M.S. degree in physics from Moscow State University, Moscow, Russia, in 2010. He is currently a senior software developer at Mirantis, Moscow, Russia. His research interests include numerical simulations, signal processing and software development for US, laser ultrasound, and photoacoustic imaging, and developing new algorithms in telecommunication technologies and cloud solutions.

Chen-wei Wei received the B.S. degree in electrical engineering from National Chiao-Tung University, Hsinchu, Taiwan, in 2003, and the M.S. and the Ph.D. degree in electrical engineering from National Taiwan University, Taipei, Taiwan, in 2005 and 2009, respectively. From 2010 to 2014, he held a postdoctoral position in bioengineering at the University of Washington, Seattle, WA, USA, working on new ultrasound and photoacoustic contrast agents and new imaging techniques. He is now a researcher/engineer in Sonavation Inc., Palm Beach Gardens, FL, USA.

Matthew O'Donnell has worked at General Electric CRD; the University of Michigan, where he was Chair of the BME Department from 1999 to 2006; and the University of Washington (UW), where he was the Frank and Julie Jungers Dean of Engineering from 2006 to 2012. He is now Professor of Bioengineering at UW. His most recent research has focused on elasticity imaging, optoacoustic arrays, photoacoustic contrast agents, thermal strain imaging, and catheter-based devices. He is a fellow of the IEEE and AIMBE and is a member of the Washington State Academy of Sciences and the National Academy of Engineering.